Impact of stresses and alloying elements on ferrous martensite nanodomains

Paul Eyméoud, Dmytro Kandaskalov, Philippe Maugis

Graphical Abstract

Impact of stresses and alloying elements on ferrous martensite nanodomains

Paul Eyméoud,Dmytro Kandaskalov,Philippe Maugis

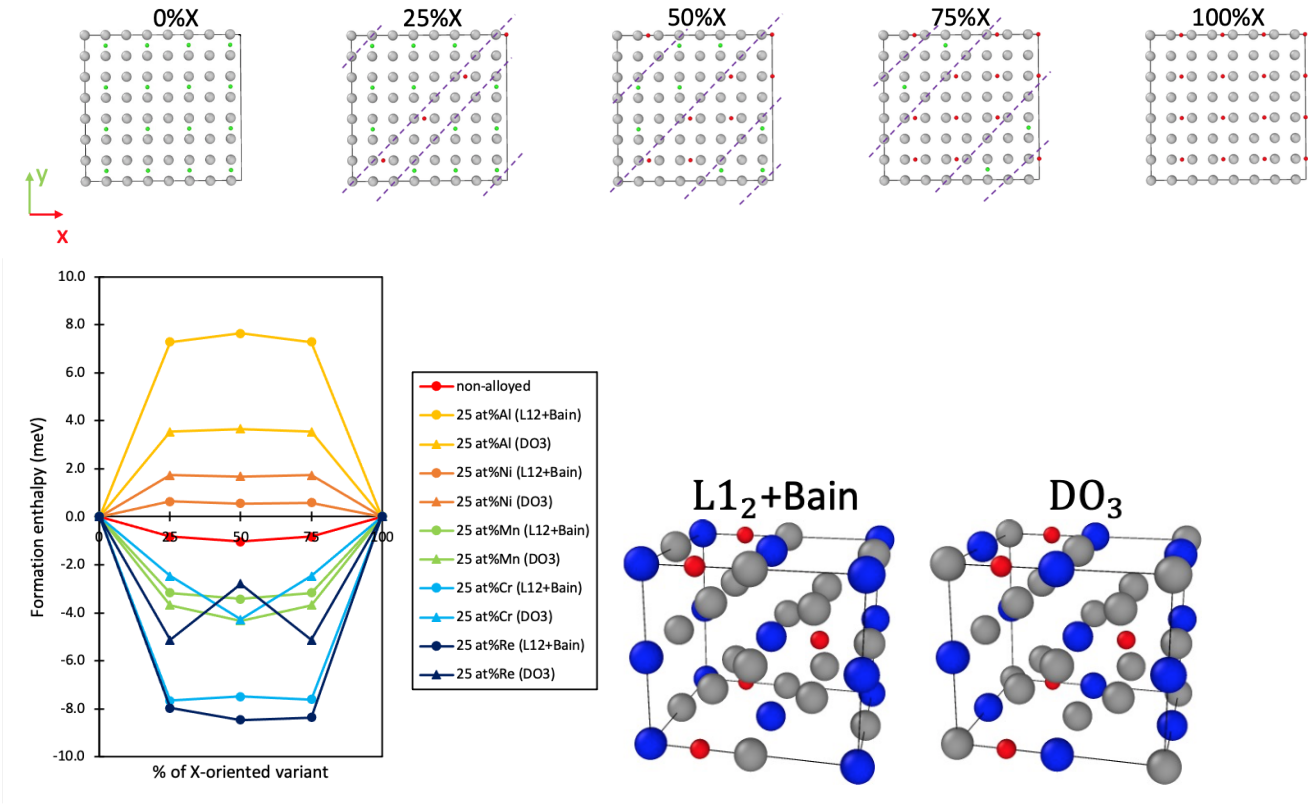

Highlights

Impact of stresses and alloying elements on ferrous martensite nanodomains

Paul Eyméoud,Dmytro Kandaskalov,Philippe Maugis

- In non-alloyed martensite, applied stress stabilizes twinned or untwinned structures.
- Twinned structures can be tetragonal oblate or orthorhombic with low tetragonality ratio.
- Ni-, Al-alloying disfavors twinning.
- Mn-, Cr-, Re-alloying favors twinning.

Impact of stresses and alloying elements on ferrous martensite nanodomains

Paul Eyméoud[a,*], Dmytro Kandaskalov[a] and Philippe Maugis[a]

[a]Aix-Marseille Univ, CNRS, IM2NP Marseille, France

ARTICLE INFO

Keywords:
Martensite
Tetragonality
Twinning
Alloying elements
Stress
Density Functional Theory

ABSTRACT

Using first-principles calculations, we investigated the impact of applied stresses and alloying elements on ferrous martensite nanodomains. In non-alloyed martensite, the procedure revealed that twinned states can be stabilized depending on applied stresses, leading to several possible crystallographic structures: body-centered tetragonal (BCT) oblate, body-centered orthorhombic (BCO), or BCT prolate. In alloyed martensite, we confirmed the experimental data from literature showing that Al or high Ni addition disfavors crystal twin formation (leading to BCT variants with high tetragonality ratios), whereas Cr, Mn, or Re addition favors crystal twin formation (leading to BCO variants with low tetragonality ratios).

1. Introduction

The crystal structure of freshly quenched ferrous martensite appears quite controversial in the literature.

In the case of non-alloyed martensite, a majority of experimental investigations [1, 2, 3, 4, 5, 6, 7] detected a body centered tetragonal (BCT) prolate host lattice occupied by iron atoms, with carbon atoms located in octahedral interstitial sites (o.i.s.). Concerning the distribution of C atoms in these o.i.s., several mean-field models [8, 9], based on elasticity theory, conclude to the stability of the so-called *Zener ordering* α', namely preferential distribution of C on one among the three o.i.s. Such particular ordering has been later confirmed by first-principles calculations [10] based on the *Special Quasirandom Structures* (SQS) technique [11].

The tetragonality ratio c/a of those non-alloyed BCT martensites has been fitted as a linear function of C content by several authors [7]. In this work, we will refer to Kurdjumov's fit [12], where p denotes mass percent of C:

$$c/a = 1 + 0.046p \tag{1}$$

However, both BCT prolate structure and equation (1) have been challenged by several sources.

First, in the simplest case of non-alloyed martensite, orthorhombic crystals with anomalously low c/a_m (with $a_m = (a + b)/2$) with respect to eq. (1) were detected by Lysak [13]. On top of that, calculations of Ruban *et al.* [14, 15], based on both first-principles and Embedded-Atom Method calculations, demonstrate the stronger thermodynamical stability of particular BCT oblate structures, with respect to Zener ordering.

Second, in the more complex case of alloyed martensite, two specific kinds of crystalline anomalies have been detected.

The first kind of crystalline anomaly, called "κ' martensite", is exactly similar to the one detected by Lysak in non-alloyed martensite [13]. It corresponds to an orthorhombic lattice with abnormally low c/a_m with respect to eq. (1), and has been detected in martensite alloyed with Cr [2], Mn [16], Re [17], and low Ni content [18].

The second kind of crystalline anomaly corresponds to a BCT prolate lattice with abnormally high c/a with respect to eq. (1), and has been detected in martensite alloyed with Al [19, 20, 21] and high Ni content [22, 23, 24].

Among the numerous investigations attempted to explain those anomalous tetragonalities [12, 24, 19, 25], starting from X-ray results [26] Kurdjumov and Khachaturyan [2, 12] demonstrated that a nano-twinning mechanism can explain the case of anomalously low tetragonalities with orthorhombicities. Following this hypothesis, we propose a first-principles investigation involving nano-twinned structures, in order to provide additional information to shed light on the link existing between martensite crystallographic changes and alloying elements.

This work is decomposed as follows. After briefly presenting our first-principles modelling techniques, we first focus on the case of non-alloyed martensite, by studying the comparative energetic stability of twinned and non-twinned configurations under several applied stresses, and associated crystalline structure. In a second part, we introduce the effect of alloying elements on host lattice, and evaluate their impact on twinning and crystalline changes.

2. Computational techniques

First-principles calculations have been performed using VASP code [27, 28] (in-house version allowing to impose stresses on cells [10]), with generalized gradient approximation [29], projector augmented wave method [30] and Perdew-Burke-Ernzerhof exchange-correlation functionals [31, 32], spin-polarized approximation, 400 eV energy cutoff, 10^{-5} eV (resp. 10^{-4} eV) for electronic self-consistency (resp. ionic relaxation criterion).

Calculations related to non-alloyed martensite (at 12.5at%C) were performed on $8 \times 8 \times 2$ BCT supercells containing 256 Fe atoms, and 32 C atoms located in o.i.s. (associated k-points representation: $2 \times 2 \times 8$ Monkhorst-Pack scheme

*Corresponding author.
paul.eymeoud@im2np.fr (P. Eyméoud)
ORCID(s): 0000-0003-4705-4244 (P. Eyméoud)

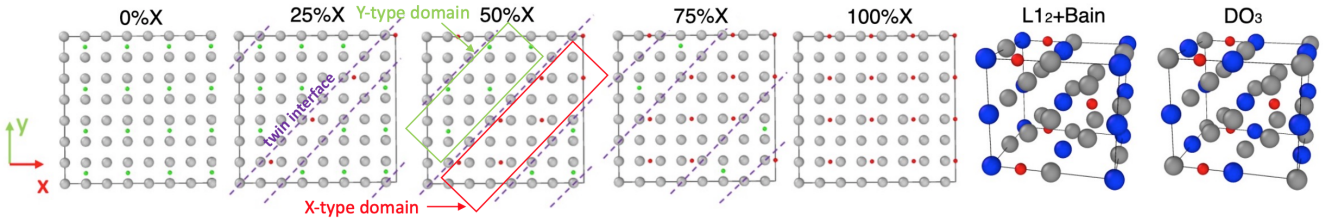

Figure 1: Supercells used for calculations: interstitial C twinning from 0% to 100% of X-type (left), and two approximations of alloying on host sublattice, transformation of $L1_2$ and DO_3 (right). Color code: grey (resp. blue) for Fe (resp. alloying element), red (resp. green) for C located in X-type (resp. Y-type) o.i.s., dashed purple for twin interfaces. For each supercell, the coordinates file is given as supplemental material.

[33]). Concerning the carbon distribution on those o.i.s., we assumed the α" distribution [34] (I4/mmm) as a rough approximation of Zener ordering α'. Such α" distribution, corresponding to a particular case of Zener ordering α', has been determined as the lowest energy distribution by DFT calculations [35], and suggested to form during spinodal decomposition using atom probe tomography [36]. What is more, choosing this α" distribution allows to avoid the time-consuming calculations on several sets of SQS necessary to represent the usual α' [10].

The nanodomains we considered are nanotwins with various proportions but same wavelength. Five different carbon distributions were studied (see Fig. 1, left): *(i)* two non-twinned distributions, namely α" ordering in X-type o.i.s. and α" ordering in Y-type o.i.s., *(ii)* three (110) twinned distributions, corresponding to 25% (resp. 75%) of C in X-type (resp. Y-type) o.i.s., 50% (resp. 50%) of C in X-type (resp. Y-type) o.i.s., and 75% (resp. 25%) of C in X-type (resp. Y-type) o.i.s.

In order to treat the case of alloyed martensite, we have approximated the 25at%M alloying case for M=Al, Ni, Cr, Mn, Re, using two different M-Fe ordered distributions on the host lattice (Fig. 1, right): *(i)* a BCT ordered repartition corresponding to $L1_2$ perovskite after Bain transformation (see Ref. [37, 19]), *(ii)* a DO_3 ordered repartition.

3. Results for non-alloyed martensite

We have computed the formation enthalpy of each of the five non-alloyed configurations of Fig. 1 left , taking for reference the non-twinned distribution with 100% of C in X-type o.i.s., using the following equation:

$$\Delta H = \Delta U - V\boldsymbol{\sigma} \cdot \Delta\boldsymbol{\epsilon}$$

wherein U denotes the internal energy, V the volume of the stress-free carbon-free crystal, $\boldsymbol{\sigma}$ (resp. $\boldsymbol{\epsilon}$) the stress (resp. strain) tensor.

We imposed a shear stress on our structures, with several amplitudes ($0\text{GPa} < \sigma_{YY} = -\sigma_{XX} < 0.5\text{GPa}$), and also a pure tension $\sigma_{YY} = 1.0\text{GPa}$ and a pure compression $\sigma_{YY} = -1.0\text{GPa}$ along (Oy). Those results, presented on Fig. 2, allow us to draw the following conclusions.

Under weak shear stress (amplitude lower than 0.075GPa), twinning stabilizes the structure. In this case, the most stable variant is the "50% of C in X-type o.i.s.", with BCT oblate crystalline structure. Such result agrees with Ruban's calculations [14, 15], stabilizing a BCT oblate structure.

Under "moderate" shear stress (amplitude between 0.075GPa and 0.225GPa), the minimum of enthalpy corresponds to the "25% of C in X-type o.i.s." twinned variant, whose crystal structure is orthorhombic with low c/a_m, in coherence with measurements from [13].

Finally, under "strong" shear stress (amplitude higher than 0.225GPa), the non-twinned variant "0% of C in X-type o.i.s." is the most stable structure, which is consistent with the aforementioned sources [1, 2, 3, 4, 5, 6, 7] claiming the stability of BCT prolate martensite, with Zener ordering.

Moreover, being conscious that, in steels, freshly formed martensite undergoes several kinds of external stresses, our computational results from Fig. 2 left can partially explain why experimentalists generally observe, without alloying elements, BCT prolate with Zener ordering, or orthorhombic with low c/a_m martensite, rather than BCT oblate martensite, which is yet numerically stabilized as particular/twinned superlattices.

Such changes of stabilities induced by shear stress are linked to the fact that tensile (resp. compressive) stress favors full Zener ordering along traction (resp. orthogonal to compression) direction, which can be seen on Fig. 2, right, in coherence with Ref. [10, 38]. On top of that, one can notice the graphical superposition between shearing $\sigma_{YY} = -\sigma_{XX} = 0.5\text{GPa}$ and pure tension $\sigma_{YY} = 1\text{GPa}$ (resp. shearing $\sigma_{YY} = -\sigma_{XX} = -0.5\text{GPa}$ and pure compression $\sigma_{YY} = -1\text{GPa}$), enhancing the preponderance of $\sigma_{YY} - \sigma_{XX}$ deviatoric part of stress tensor.

Although the previous results are based on a specific carbon distribution in o.i.s. (α"), its validity can be generalized, since the α" distribution is a particular case (lowest-energy distribution [35]) of the more general α' one. By replacing the set of α" twinned and non-twinned ordered variants of Fig. 1 by several sets of α' twinned and non-twinned disordered SQS [10], one can reach, after averaging, the same stability results presented on Fig. 2, provided that the number of SQS is sufficient.

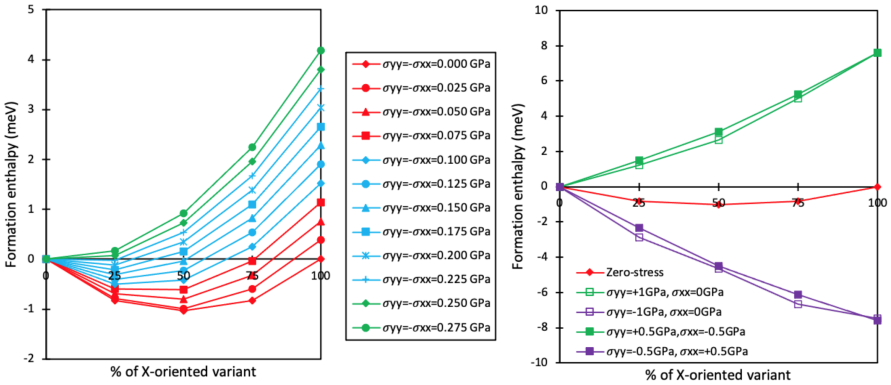

Figure 2: Crystal twin formation enthalpy in non-alloyed martensite (reference: 0%X variant taken under same stress). Left: under shear stress (color code denotes, for each plot, the minimum enthalpy: red for BCT oblate 50%X variant, blue for orthorhombic 25%X variant, and green for BCT prolate 0%X variant). Right: under shear, tensile and compressive stress.

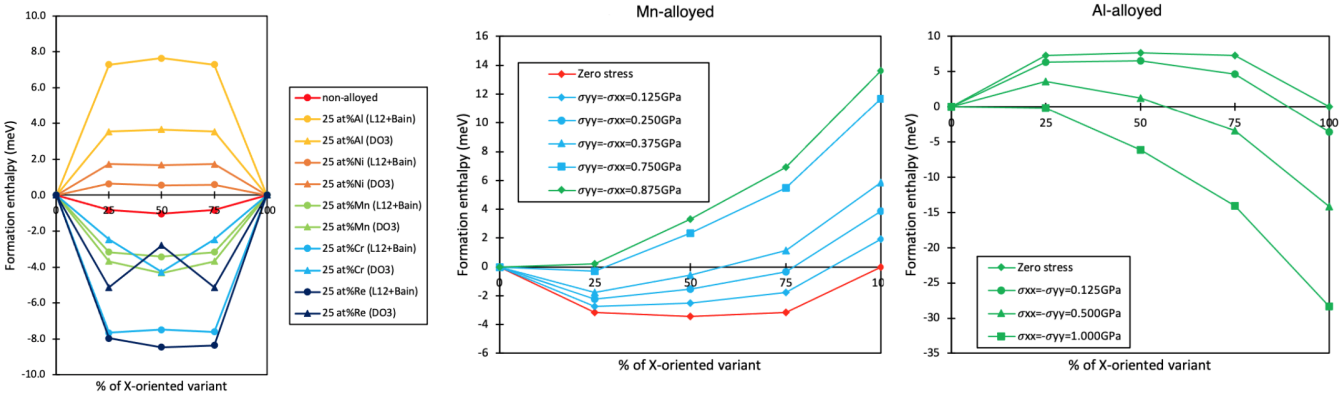

Figure 3: Crystal twin formation enthalpy for alloyed martensite (reference: 0%X variant taken under same stress). Left: under zero stress. Center (resp. right): case of Mn-alloyed (resp. Al-alloyed) martensite, under imposed shear stress.

4. Results for alloyed martensite

We have computed, at zero stress, the formation enthalpy of each configuration of Fig. 1, in the alloyed case. For that, we have changed the iron host lattice by a Fe-M host lattice at 25at%M, using two kinds of approximations to represent alloying (cf. Section 2).

The results, presented on Fig. 3, left, allow us to split the alloying elements in two categories, depending on formation enthalpy sign: Mn, Cr, or Re addition energetically favors twinning, whereas Al or Ni addition energetically disfavors twinning (strongly for Al, and slightly for Ni). An important point is the fact that both ordered host lattices (L12+Bain and DO3) lead to the same dichotomy (Al, Ni on the one side, and Cr, Mn, Re on the other side), despite their strong symmetry difference (in carbon-free case, L12+Bain is BCT, and DO3, BCC). Therefore, we can assume that the classification "Al, Ni versus Cr, Mn, Re" does not depend on host lattice symmetry or ordering, and is thus valid for any other alloying element distribution on host lattice.

Moreover, if one applies a shear stress on those alloyed martensite structures, two situations can occur depending on the alloying element employed: *(i)* for Mn-, Cr- or Re-alloyed martensite, the crystallographic behavior is the same than non-alloyed martensite (cf. Fig. 3, center), namely BCT oblate structure under weak stress, orthorhombic with low c/a_m under moderate stress, and BCT prolate under strong stress, *(ii)* for Al- and Ni-alloyed martensite, the most stable structure remains the BCT prolate one without twins, whatever the amplitude of imposed shear stress (cf. Fig. 3, right).

Such dichotomy (non-alloyed, Mn, Cr, Re versus Al and Ni) matches very well the experimental observations from literature. On the one hand, the orthorhombic lattice with low c/a_m detected in non-alloyed, Mn-, Cr- and Re-alloyed martensite results from presence of twins. On the other hand, the BCT prolate lattice detected in Al- and high-Ni- alloyed crystals is caused by the absence of twins, and the associated abnormally high c/a results from the host lattice softening induced by alloying elements [35]. Moreover, in the specific case of Ni, the *slight* tendency to disfavor twinning appearing on Fig. 3 left coincides with the ambivalent observations on Ni-alloyed martensite depending on Ni concentration: tendency to form orthorhombic structures with low c/a_m at low at%Ni [18] (situation close to the non-alloyed red plot on Fig. 3 left), versus tendency to form BCT prolate structures

with high c/a at high at%Ni [22, 23, 24] (situation close to the 25at%Ni-alloyed orange plots on Fig. 3 left).

5. Conclusion

Using first-principles calculations, we have compared the thermodynamic stabilities of twinned martensite structures with respect to non-twinned ones.

In the non-alloyed case, we have managed to reconciliate the controversial data from literature concerning non-alloyed martensite crystalline changes. Because of twinning, the theoretical most stable structure at zero stress appears to be BCT oblate, in coherence with Ruban's calculations [14, 15]. However, since freshly formed martensite undergoes several kinds of stresses, experimentalists almost always observe BCT prolate structures with Zener ordering [1, 2, 3, 4, 5, 6, 7], that are most stable under strong applied stresses which disfavor twinning. Nethertheless, in some cases where the applied stresses are moderate, some twinned orthorhombic structures with low c/a_m can be detected [13].

In the alloyed case, we explained the two kinds of crystalline anomalies found in literature [12] and confirm their twinning origin. On the one side, Mn-, Cr-, and Re-alloying favors twinning, leading, under applied stresses, to orthorhombic structures with low c/a_m ratios. On the other side, Ni- and Al-alloying disfavors twinning whatever the applied stress, leading to BCT prolate structures with high c/a ratios.

Acknowledgments, Data availability statement

This work was supported by the Agence Nationale de la Recherche (contract C-TRAM ANR-18-CE92-0021). Centre de Calcul Intensif d'Aix-Marseille is acknowledged for granting access to its high performance computing resources. Paul Eyméoud thanks Armen Khachaturyan for fruitful discussions, and Damien Connétable for sharing his VASP in-house version allowing to impose stresses on supercells.

Data are available upon request.

CRediT authorship contribution statement

Paul Eyméoud: Conceptualization, Methodology, Software, Writing - Original Draft, Writing - Review and Editing. **Dmytro Kandaskalov:** Methodology. **Philippe Maugis:** Supervision.

References

[1] W. L. Fink and E. D. Campbell *Trans. Am. Soc. Steel Treat.*, vol. 9, p. 717, 1926. https://books.google.fr/books/about/Influence_of_Heat_Treatment_and_Carbon_C.html?id=AotBAAAAIAAJ&redir_esc=y.

[2] G. Kurdjumov and A. Khachaturyan *Acta Metallurgica*, vol. 23, pp. 1077–1088, 1975. https://doi.org/10.1016/0001-6160(75)90112-1.

[3] Y. Wang, Y. Tomota, T. Ohmura, S. Morooka, W. Gong, and S. Harjo *Acta Materialia*, vol. 184, pp. 30–40, 2020. https://doi.org/10.1016/j.actamat.2019.11.051.

[4] S. Nagakura, Y. Hirotsu, M. Kusunoki, T. Suzuki, and Y. Nakamura *Metallurgical Transactions A*, vol. 14A, pp. 1025–1031, 1983. https://doi.org/10.1007/BF02670441.

[5] Z. Fan, L. Xiao, Z. Jinxiu, K. Mokuang, and G. Zhenqi *Physical Review B*, vol. 52, no. 14, pp. 9979–9987, 1995. https://doi.org/10.1103/PhysRevB.52.9979.

[6] O. D. Sherby, J. Wadsworth, D. Lesuer, and C. Syn *Material Science Forum*, vol. 539-543, pp. 215–222, 2007. https://doi.org/10.4028/www.scientific.net/MSF.539-543.215.

[7] L. Cheng, A. Bottger, T. H. de Keijser, and E. Mittemeijer *Scripta Metallurgica et Materialia*, vol. 24, pp. 509–514, 1990. https://doi.org/10.1016/0956-716X(90)90192-J.

[8] C. Zener *Phys. Rev.*, vol. 74, no. 6, pp. 639–647, 1948. https://doi.org/10.1103/PhysRev.74.639.

[9] P. Maugis *Acta Materialia*, vol. 158, pp. 454–465, 2018. https://doi.org/10.1016/j.actamat.2018.08.001.

[10] P. Maugis, D. Connétable, and P. Eyméoud *Scripta Materialia*, vol. 194, p. 113632, 2021. https://doi.org/10.1016/j.scriptamat.2020.113632.

[11] A. Zunger, S.-H. Wei, L. G. Ferreira, and J. E. Bernard *Physical Review Letters*, vol. 65, no. 3, pp. 353–356, 1990. https://doi.org/10.1103/PhysRevLett.65.353.

[12] G. Kurdjumov *Metallurgical Transactions A*, vol. 7, no. 7, pp. 999–1011, 1976. https://doi.org/10.1007/BF02644066.

[13] L. I. Lysak and Y. N. Vovk *Fizika Metallov Metallovedenie*, vol. 31, p. 646, 1971. https://scholar.google.com/scholar?hl=fr&as_sdt=0%2C5&q=Lysak+Vovk+Fizika+Metallov+Metallovedenie+1971&btnG=.

[14] A. V. Ruban *Physical Review B*, vol. 90, no. 14, p. 144106, 2014. https://doi.org/10.1103/PhysRevB.90.144106.

[15] J. Y. Yan and A. V. Ruban *Computational Materials Science*, vol. 147, pp. 293–303, 2018. https://doi.org/10.1016/j.commatsci.2018.02.024.

[16] L. I. Lysak, J. N. Vovk, and J. M. Polishchuk *Fizika Metallov Metallovedenie*, vol. 23, p. 898, 1967. http://impo.imp.uran.ru/fmm/Electron/vol23_5/abstract18.pdf.

[17] L. I. Lysak and L. O. Andrushchik *Fizika Metallov Metallovedenie*, vol. 28, p. 348, 1969. http://impo.imp.uran.ru/fmm/Electron/VOL28_2/abstract25.pdf.

[18] L. I. Lysak and V. E. Danilchenko *Physics of Metals and Metallography*, vol. 32, p. 194, 1971. https://scholar.google.com/citations?view_op=view_citation&hl=en&user=AwypNzsAAAAJ&citation_for_view=AwypNzsAAAAJ:u-x6o8ySG0sC.

[19] S. Uehara, S. Kajiwara, and T. Kikuchi *Materials Transactions JIM*, vol. 33,3, p. 220, 1992. https://doi.org/10.2320/matertrans1989.33.220.

[20] M. Watanabo and C. M. Wayman *Scripta Metallurgica*, vol. 5, p. 109, 1972. https://doi.org/10.1016/0036-9748(71)90040-8.

[21] G. V. Kurdjumov, V. K. Kristskaya, and V. A. Ilina *Doklady Akademii Nauk SSSR*, vol. 219, p. 1099, 1974. https://inis.iaea.org/search/search.aspx?orig_q=RN:6209404.

[22] L. I. Lyssak, S. A. Artimiuk, and J. M. Polishchuk *Fizika Metallov i Metallovedenie*, vol. 35, p. 1098, 1973. https://inis.iaea.org/search/searchsinglerecord.aspx?recordsFor=SingleRecord&RN=4084947.

[23] G. V. Kurdjumov, L. K. Mikhailova, and A. G. Khachaturyan *Doklady Akademii Nauk SSSR*, vol. 215, p. 578, 1974. https://www.researchgate.net/publication/253288965_Anomalously_high_tetragonality_of_martensite_with_high_nickel_content_and_the_nature_of_the_anomalies_of_the_tetragonality.

[24] S. Kajiwara and T. Kikuchi *Acta Metallurgica et Materialia*, vol. 39, p. 1123, 1991. https://doi.org/10.1016/0956-7151(91)90200-K.

[25] J. W. Christian *Materials Transactions JIM*, vol. 33, p. 208, 1992. https://doi.org/10.2320/matertrans1989.33.208.

[26] L. I. Lysak, S. P. Kondratiev, and J. M. Polishchuk *Fizika Metallov Metallovedenie*, vol. 36, p. 546, 1973. https://scholar.google.com/scholar?hl=fr&as_sdt=0%2C5&q=Dependence+of+the+Crystal+Structure+of+Kappa-Prime+and+Alpha-Martensites+on+C+Content&btnG=.

[27] G. Kresse and J. Furthmüller *Computational Materials Science*, vol. 6, p. 15, 1996. https://doi.org/10.1016/0927-0256(96)00008-0.
[28] G. Kresse and J. Furthmüller *Physical Review B*, vol. 54, p. 11169, 1996. https://doi.org/10.1103/PhysRevB.54.11169.
[29] G. Kresse and D. Joubert *Physical Review B*, vol. 59, p. 1758, 1999. https://doi.org/10.1103/PhysRevB.59.1758.
[30] P. E. Blöchl *Physical Review B*, vol. 50, p. 17953, 1994. https://doi.org/10.1103/PhysRevB.50.17953.
[31] J. P. Perdew, K. Burke, and M. Ernzerhof *Physical Review Letters*, vol. 77, p. 3865, 1996. https://doi.org/10.1103/PhysRevLett.77.3865.
[32] J. P. Perdew, K. Burke, and M. Ernzerhof *Physical Review Letters*, vol. 78, p. 1396, 1997. https://doi.org/10.1103/PhysRevLett.78.1396.
[33] H. J. Monkhorst and J. D. Pack *Physical Review B*, vol. 13, p. 5188, 1976. https://doi.org/10.1103/PhysRevB.13.5188.
[34] K. H. Jack *Proceedings of the Royal Society A*, vol. 208, p. 216, 1951. https://doi.org/10.1098/rspa.1951.0155.
[35] S. Chentouf, S. Cazottes, F. Danoix, M. Goune, H. Zapolsky, and P. Maugis *Intermetallics*, vol. 89, pp. 92–99, 2017. https://doi.org/10.1016/j.intermet.2017.05.022.
[36] P. Maugis, F. Danoix, M. Dumont, S. Curelea, S. Cazottes, H. Zapolsky, and M. Gouné *Materials Letters*, vol. 214, p. 213, 2018. https://doi.org/10.1016/j.matlet.2017.12.007.
[37] R. Oshima and C. M. Wayman *Metallurgical Transactions*, vol. 3, p. 2163, 1972. https://doi.org/10.1007/BF02643228.
[38] P. Maugis *Journal of Phase Equilibria and Diffusion*, vol. 41, pp. 269–275, 2020. https://doi.org/10.1007/s11669-020-00816-2.